The Neutral Lipid Composition Present in the Digestive Vacuole of *Plasmodium falciparum* Concentrates Heme and Mediates β-Hematin Formation with an Unusually Low Activation Energy[†]

Anh N. Hoang,[‡] Rebecca D. Sandlin,[‡] Aneesa Omar,[§] Timothy J. Egan,*[,§] and David W. Wright*[,‡]

[‡]*Department of Chemistry, Vanderbilt University, Station B351822, Nashville, Tennessee 37235, United States, and*
[§]*Department of Chemistry, University of Cape Town, Private Bag, Rondebosch 7701, South Africa*

Received August 30, 2010; Revised Manuscript Received October 23, 2010

ABSTRACT: In eukaryotic cells, neutral lipids serve as major energy storage molecules; however, in *Plasmodium falciparum*, a parasite responsible for causing malaria in humans, neutral lipids may have other functions during the intraerythrocytic stage of the parasite life cycle. Specifically, experimental data suggest that neutral lipid structures behave as a catalyst for the crystallization of hemozoin, a detoxification byproduct of several blood-feeding organisms, including malaria parasites. Synthetic neutral lipid droplets (SNLDs) were produced by depositing a lipid blend solution comprised of mono- and diglycerides onto an aqueous surface. These lipid droplets are able to mediate the production of brown pigments that are morphologically and chemically identical to hemozoin. The partitioning of heme into these SNLDs was examined by employing Nile Red, a lipid specific dye. Soluble ferriprotoporphyrin IX was observed to spontaneously localize to the lipid droplets, partitioning in a pH-dependent manner with an estimated log P of 2.6. Interestingly, the pH profile of heme partitioning closely resembles that of β-hematin formation. Differential scanning calorimetry and kinetic studies demonstrated that the SNLDs provide a unique environment that promotes hemozoin formation. SNLD-mediated formation of the malaria pigment displayed an activation energy barrier lower than those of individual lipid components. In particular, lipid droplets composed of diglycerides displayed activation barriers lower than those composed of monoglycerides. This difference was attributed to the greater fluidity of these lipids. In conjunction with the known pattern of lipid body proliferation, it is suggested that neutral lipid structures within the digestive vacuole not only are the location of in vivo hemozoin formation but are also essential for the survival of the parasite by functioning as a kinetically competent and site specific mediator for heme detoxification.

Intracellular neutral lipid particles or macromolecular lipid assemblies are present in nearly all organisms (*1*). Generally, these particles function as storage compartments and metabolic organelles (reviewed in ref *1*). However, in *Plasmodium*, neutral lipids are hypothesized to exhibit an unusual function in the parasite heme detoxification pathway. During the blood stage of the infection, the parasite enters the host erythrocyte and degrades hemoglobin as a source of nutrients (*2, 3*) and possibly also both to create space (*4*) within the cell and to maintain osmotic balance (*5−7*). As a consequence of hemoglobin catabolism, toxic free heme, in near molar concentrations, is released within the acidic digestive vacuole (DV)[1] (*8*). The parasite circumvents this toxicity by quickly sequestering the heme into a crystal known as hemozoin. Hemozoin is morphologically and chemically

identical (*9−11*) to its synthetic form, β-hematin, although a recent study has indicated that there are subtle differences between natural hemozoin and β-hematin prepared under non-aqueous equilibrium conditions. The former appears to exhibit more disorder in the Fe−O bonds than the latter (*12*). It is a microcrystalline cyclic dimer of ferriprotoporphyrin IX [Fe(III)PPIX] in which the propionate side chain of one protoporphyrin coordinates to the iron(III) center of the other and protoporphyrin molecules interact via significant π-stacking interactions of their unligated faces (*12, 13*). The dimers hydrogen bond to their neighbors via the second propionic acid group, forming extended chains through the crystal. Though hemozoin has been exhaustively characterized, the mechanism responsible for its formation remains a topic of debate. Furthermore, it is believed that this process is inhibited by chloroquine and other quinoline and related antimalarials (*14*). In view of the continued emergence of drug resistance, a more detailed understanding of hemozoin crystallization may facilitate development of future treatments that target this parasite specific pathway.

The dramatic increase in the lipid content of the infected erythrocyte (*15−19*) and observations of hemozoin localization in neutral lipid "nanospheres" or their proximity to membranous structures thought to be remnants of the inner membrane of transport vesicles (TVs) involved in hemoglobin ingestion (*20−22*) have directed investigations of hemozoin formation toward

[1]Abbreviations: SNLD, synthetic neutral lipid droplet; DSC, differential scanning calorimetry; DV, digestive vacuole; Fe(III)PPIX, ferriprotoporphyrin IX; TV, transport vesicle; NLB, neutral lipid body; TAG, triacylglycerol; DAG, diacylglycerol; MSG, monostearoylglycerol; MPG, monopalmitoylglycerol; DOG, 1,3-dioleoylglycerol; DPG, 1,3-dipalmitoylglycerol; DLG, 1,3-dilinoleoylglycerol; NR, Nile Red; pXRD, powder X-ray diffraction; SEM, scanning electron microscopy; TEM, transmission electron microscopy.

neutral lipids. Specifically, triacylglycerol (TAG) and diacylglycerol (DAG), lipids traditionally important for membrane biogenesis and energy storage, are synthesized by *Plasmodium falciparum* and packaged into neutral lipid bodies (NLBs) in a stage specific manner within the DV (*17, 18, 23*). In contrast, these lipids are barely detectable in uninfected erythrocytes (*15, 19*). The NLBs are closely associated with the DV and have been suggested to ultimately derive from digestion of TV phospholipids in the DV. However, the function of NLBs during parasite growth remains unclear. Two popular hypotheses include NLBs functioning as a depot of lipid intermediates that are generated during digestion of phospholipids (*23*) and NLBs serving as a deposit of lipid components that can be quickly mobilized to supply the growing parasite with fatty acids and acylglycerols for membrane generation (*18*). In this study, experimental data suggest that these neutral lipids function as a mediator of hemozoin formation in a site and time specific manner.

Recently, Pisciotta et al. reported that a specific blend of mono-, di-, and triacylglycerols present in the DV is sufficient for mediating hemozoin formation (*21*). Thin layer chromatography together with mass spectrometry identified the components of these lipids to be the monoglycerides monostearoylglycerol (MSG) and monopalmitoylglycerol (MPG) and the diglycerides 1,3-dioleoylglycerol (DOG), 1,3-dipalmitoylglycerol (DPG), and 1,3-dilinoleoylglycerol (DLG) in a 4:2:1:1:1 ratio (*21*). Here, SNLDs comprising the same ratio as this biological lipid blend were utilized to investigate the localization and partitioning of Fe(III)PPIX into the lipid droplets. DSC and kinetic measurements demonstrate that the lipid blend provides a unique environment for hemozoin formation. Via observation of the collisional (Stern−Volmer) quenching of Nile Red (NR) fluorescence, confocal microscopy and conventional fluorescence spectroscopy reveal that soluble Fe(III)PPIX rapidly localizes to the SNLDs and partitions into SNLDs in a pH-dependent manner. In conjunction with the known pattern of lipid body proliferation, it is proposed that neutral lipids, possibly precursors related to NLBs, are both the mediator and location of in vivo hemozoin formation.

EXPERIMENTAL PROCEDURES

Reagents. All lipids were obtained from Nu-Check prep inc. (Elysian, MN) or Sigma-Aldrich (Vorna Valley, South Africa). The lipid blend refers to the established 4:2:1:1:1 MSG:MPG:DOG:DLG:DPG biological ratio reported by the Sullivan group (*21*). Each lipid was dissolved in a 9:1 mixture of methanol and acetone to promote lipid solubility. Stock solutions of lipid were prepared at 16.2 mM. Porcine hematin (Sigma or Fluka) was prepared by dissolving the solid in 0.1 M NaOH with vortexing for 2 min followed by addition of a 9:1 methanol/acetone mixture such that the desired concentration is achieved in a 1:1 mixture of the NaOH solution and the methanol/acetone solution. We prepared citric buffer by dissolving citric acid at 50 mM and adjusting to the desired pH, usually 4.8, using NaOH. A 20 μM stock solution of NR (MP Biomedicals, LLC, or Sigma-Aldrich) was prepared in acetone and used immediately.

Characterization. (*i*) *Formation and Characterization of SNLDs*. A Malvern Zetasizer with a lower limit of 0.6 nm and an upper limit of 6 μm was utilized in the size stability and ζ potential measurements of the neutral lipid particles. A sample was prepared by depositing the lipid (in a 9:1 methanol/acetone

mixture) onto the citric buffer and immersed in a 37 °C water bath to allow the formation of a lipid emulsion to take place. A 22.5 gauge needle was then used to extract samples for measurement by carefully removing the bulk lipid subphase while avoiding withdrawal of the surface lipid monolayer. This technique was repeated for each lipid. The SNLDs were further characterized using confocal microscopy to visually confirm that the lipid particles exhibit continuous as opposed to hollow interiors (i.e., are droplets rather than liposomes). SNLD preparation for confocal imaging is described in the Fe(III)PPIX partitioning section below.

(*ii*) *Differential Scanning Calorimetry (DSC)*. Thermal analysis (TA) of neutral lipid samples encapsulated in sealed aluminum capsules was conducted with a TA Instruments DSC Q200. Approximately 2.4−3.2 mg samples of each lipid were weighed with a microbalance and analyzed over a temperature range from 80 to −80 °C at a cooling rate of 10 °C/min and a heating rate of 15 °C/min. The exothermic and endothermic peaks were determined by plotting heat flow (adjusted for weight) versus temperature.

(*iii*) *β-Hematin Characterization*. Products collected from depositing premixed neutral lipid blend (*21*) with Fe(III)PPIX in a 9 cm Schott-Duran crystallization dish were characterized to confirm the presence of β-hematin. Fourier transform infrared (FTIR) spectroscopy was used to characterize the product β-hematin formed in the lipid/water system. The product was washed extensively using a 5% pyridine solution and further characterized using powder X-ray diffraction (pXRD). pXRD was conducted using Cu Kα radiation (λ = 1.541 Å), with data collection on a Philips PW1050/80 vertical goniometer in the 2θ range of 5−40° using an Al sample holder. Images of crystal products were obtained on a Hitachi S-4200 scanning electron microscope (SEM). Lattice spacings were measured from images obtained from a Philips CM20 transmission electron microscope (TEM).

Fe(III)PPIX Localization and Partitioning into Synthetic Neutral Lipid Droplets.   (*i*) *Nile Red Fluorescence Quenching by Fe(III)PPIX*. Fluorescence spectra of NR (*24*) were recorded in acetone as a function of concentration to determine the linear range of intensity versus concentration. A series of fluorescence spectra were also recorded in different solvents to observe the dependence of λ_{em}(max) on polarity. To observe the effects of Fe(III)PPIX on NR fluorescence, a 100:1 lipid/NR solution was prepared with a final concentration in buffer at the desired pH of 100 μM lipid and 1.0 μM NR. The following buffers were used: 0.020 M HEPES [4-(2-hydroxyethyl)-1-piperazineethanesulfonic acid] at pH 6.0−8.0 or citric acid/citrate at pH 2.8−5.5. A 1 mL aliquot of NR-labeled SNLD dispersed in aqueous medium was placed in a quartz fluorescence cuvette and titrated with Fe(III)PPIX prepared by dissolving hematin in 0.1 M NaOH. The fluorescence spectrum was measured on a Varian Cary Eclipse fluorescence spectrophotometer. Both excitation and emission slit widths were set to 5 nm with a medium scan control and medium PMT detector voltage. The sample was excited at 540 nm, and the emission spectrum was recorded from 560 to 800 nm.

Data were analyzed according to the Stern−Volmer equation (eq 1) (*25*):

$$\frac{I_0}{I} = 1 + K_{SV}[Q] \tag{1}$$

where I_0 is the intensity at λ_{em}(max) in the absence of the quencher, I is the observed intensity at λ_{em}(max) in the presence

of a given concentration of quencher, K_{SV} is the Stern–Volmer quenching constant, and [Q] is the concentration of the quencher, in this case Fe(III)PPIX.

Partitioning of Fe(III)PPIX between an aqueous solution and octanol was measured at pH 7.51 using a HEPES-buffered aqueous solution (0.020 M, 3 mL). The Fe(III)PPIX stock solution (500 μM) was prepared from hematin in MeOH and then introduced into the buffer at a final concentration of 57.8 μM. This was shaken and equilibrated for 6 h at 37 °C with an equal volume of octanol. At the end, the UV–visible spectra of the aqueous and octanol layers were recorded on a Varian Cary 100 spectrophotometer at 403 nm.

(*ii*) *Confocal Microscopy Studies.* For confocal micros-copy measurements, the 16.2 mM lipid blend solution was prepared using stocks in a 4:2:1:1:1 volume ratio. We prepared a 100:1 lipid/NR solution by combining 150 μL of NR stock with 18.5 μL of lipid blend stock. This solution was briefly vortexed and diluted with a 50 mM solution of citric buffer (pH 4.8) to give a final volume of 1 mL. This solution was again briefly vortexed, giving a final lipid concentration of 300 μM and an NR concentration of 3 μM. A lipid volume of 180 μL was imaged in a glass bottom microwell dish (35 mm Petri dish and 14 mm microwell dish, MatTek Corp.). A 500 μM Fe(III)PPIX solution was prepared for quenching of the NR signal as described above. Quenching was performed by sequentially adding 20 μL of the Fe(III)PPIX solution every ~30 s, starting 10 s into imaging, until complete quenching was observed. Great care was taken not to displace the lipid droplets. Measurements were taken using a Zeiss LSM 510META upright confocal microscope (VUMC Cell Imaging Shared Resource) using the time series application with 63× oil (1.4) immersion objectives. Z stacking was performed before and after quenching to ensure lipid droplets were not displaced during the experiment. The quenching experiment was repeated with the exception of introducing 400 μL of 250 μM Fe(III)PPIX at once (10 s into imaging). The quenching experi-ments were repeated for citric buffer adjusted to pH 1.3, 2.3, 4.8, 5.5, 6.7, 7.3, and 8.1. The rate of photobleaching was measured by imaging the fluorescence intensity of NR-labeled SNLDs in the absence of heme for 200 s. The experiment was repeated for pH 4.8 with the addition of 140 μL of Fe(III)PPIX.

Kinetics of β-Hematin Formation. Kinetics were per-formed using a method that we have previously optimized with respect to yield, rate, and reproducibility and which has been reported in detail (*26*). Reactions were performed at pH 4.8 in 15 mL Falcon polypropylene conical tubes. After equilibration for ~15 min in a Thermo Precision reciprocal shaking water bath, samples were carefully but quickly deposited (dropwise) onto the surface of the citric buffer using a 1 mL syringe with a 22.5 gauge needle. Extreme care was taken not to disturb the solution within the tube. All data sets were completed in triplicate and at four distinct temperatures ranging from 25 to 60 °C. Activation energies were calculated by fitting experimental data to the Arrhenius equation. Statistical analysis (*t* test) was performed using GraphPad Prism version 4.0.

RESULTS

Characterization of β-Hematin. Structural, spectroscopic, and morphological analyses of the brown pigment formed by introduction of soluble Fe(III)PPIX into the lipid blend emulsion of SNLDs unequivocally confirm the formation of β-hematin (Figure 1). pXRD exhibits the three strong and numerous weaker
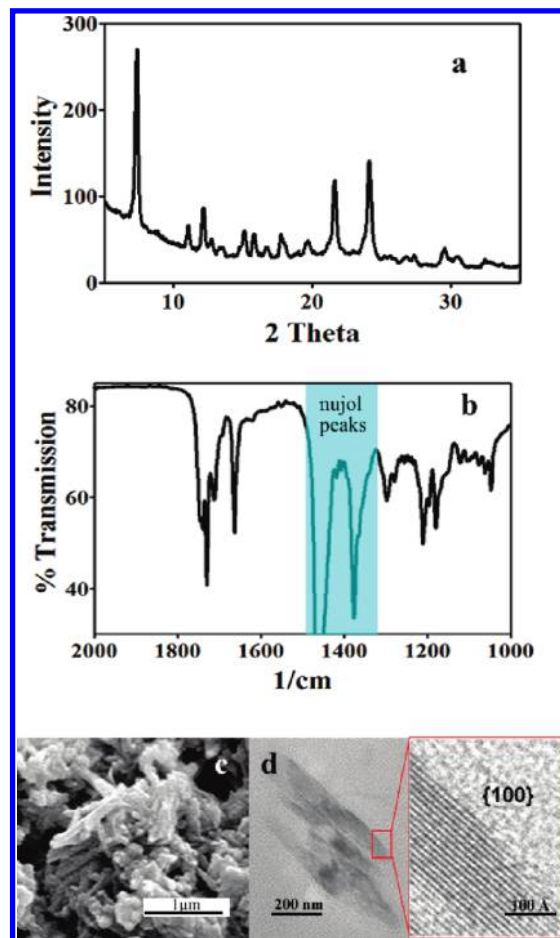

FIGURE 1: Characterization of β-hematin produced using SNLDs suspended in citric buffer (pH 4.8) at 37 °C. (a) pXRD, (b) FTIR, (c) SEM, and (d) TEM data all show the characteristic features of β-hematin. Fringes in the TEM image in panel d exhibit a lattice spacing of 13.4 ± 1 Å, corresponding to β-hematin characteristic pXRD peaks at approximately 7.6 ± 0.5 2θ, close to that seen in panel a.

diffraction peaks characteristic of β-hematin (Figure 1a). Infra-red spectra exhibiting prominent peaks at 1662 and 1210 cm^{-1}, corresponding to the presence of the C=O and C–O stretching vibrations of propionate-linked hematin dimers, respectively, further confirm the formation of β-hematin (Figure 1b). SEM of the product showed needlelike crystals resembling hemozoin in crystal habit (Figure 1c), while TEM of the largest face displayed electron dense crystals with a lattice spacing close to that expected for the {100} face of hemozoin (Figure 1d). Collectively, these findings definitively confirm the ability of SNLDs to mediate β-hematin formation.

Characterization of Synthetic Neutral Lipid Droplets. The SNLDs were formed by depositing a 9:1 methanol/acetone solution of the neutral lipid blend onto an aqueous layer. Confocal imaging of samples extracted from just beneath the surface confirmed that this composition of lipids spontaneously organizes into an emulsion (Figure 2). Orthogonal projections of these lipid droplets demonstrate formation of spherical lipid droplets with continuous, nonhollow interiors (Figure 2a), similar to our previously reported study using pure monoglyceride (*26*). Visually, the SNLDs exhibited a size distribution of a few hundred nanometers to few micrometers in diameter. In addition to confocal microscopic observations, the ζ potentials of the blend and its individual components were compared in an effort to explore the possibility that cations might accumulate around
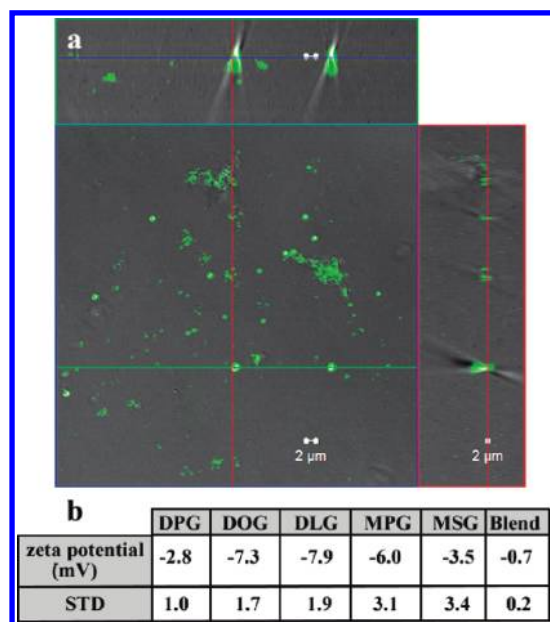
Figure 2: Confocal micrographs of SNLDs and ζ potentials of SNLDs and droplets composed of component lipids. (a) Confocal microscopy of NR-labeled SNLDs composed of the 4:2:1:1:1 MSG/MPG/DOG/DLG/DPG lipid blend demonstrates the presence of micrometer-sized lipid droplets with continuous interiors. (b) ζ potentials and standard deviations (STD) of the individual neutral lipids and the blend show that they are all close to zero as expected.

the headgroups. However, true to their "neutral" lipid definition, no significant charge potential difference was observed for each individual component or the lipid blend composition (Figure 2b). Conventionally, ζ potential values higher than an absolute value of 25 mV are considered typical of stable colloids because of the electrostatic repulsion between particles, while colloids with ζ potentials with absolute values of < 10 mV tend to flocculate or coalesce because surface charge is negligible (*27, 28*). By comparison, ζ potential values for liposomes made of 1,2-dioleoyl-3-trimethylammoniopropane (DOTAP) and 1,2-dioleoyl-*sn*-glycerol-3-phosphoethanolamine (DOPE) at room temperature are 50 mV (*29*). A final point to note is that we cannot be sure that all of the SNLDs have the same composition as the bulk lipid solution from which they are formed. It is possible that they may represent a heterogeneous population, so observations reported may represent an average behavior of the sample.

To determine whether the lipid blend has unique properties different from those of its individual components, DSC was performed on the blend and on the component lipids. Ideally, if the heterogeneous lipid composition of the blend provides better packing of lipid molecules through new intermolecular interactions, a detectable change in heat flux would be necessary to break these new interactions. Measured phase transition peaks of the five neutral lipid samples were consistent with those of published values (*30*). Lipids containing saturated hydrocarbon chains (MSG, MPG, and DPG) have a higher melting point than lipids with unsaturated chains (DLG and DOG). When the saturated lipids MSG, MPG and DPG were heated, negative heat flow peaks were measured at 76, 74, and 74 °C, respectively (Figure 3a−c). These values matched those of published measurements (*30, 31*) for corresponding melting temperatures. Cooling of the samples produced a positive heat flow at 69, 63, and 63 °C, respectively, corresponding to crystallization peaks of MSG, MPG, and DPG, respectively. In general, pure saturated
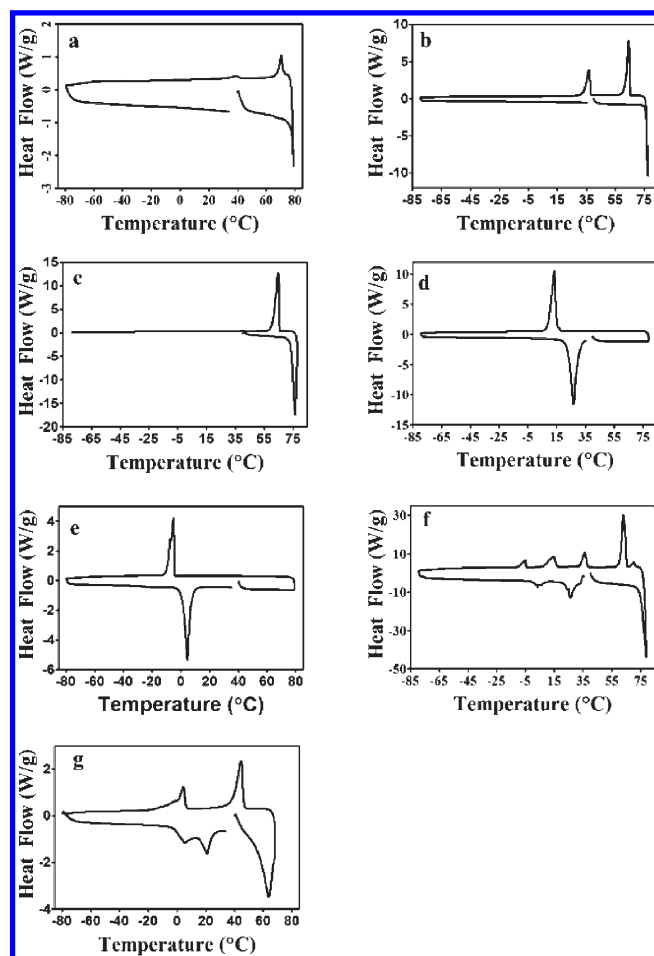

Figure 3: DSC of individual lipids and the lipid blend. The scans are for (a) MSG, (b) MPG, (c) DPG, (d) DOG, (e) DLG, (f) an MSG/MPG/DOG/DLG/DPG overlay with components normalized to the lipid blend ratio of 4:2:1:1:1, and (g) the lipid blend.

asymmetric monoglycerides exist in three polymorphic forms, namely, sub-α, α, and β (*32*). All polymorphs have a double chain length packing mode, characterized by a long spacing of ~50 Å for MSG (*32*). When monoglycerides, present in the α polymorph, are cooled 35−50 °C below the crystallization point, they undergo a polymorphic transition to a reversible sub-α polymorph. Further cooling of MSG and MPG samples produced positive heat flow peaks at 40 and 36 °C. These peaks are interpreted as the transition point (α to sub-α form) for MSG and MPG and are consistent with transition temperatures published by Gunston and Padley (*30*).

Phase transition measurements for unsaturated diglycerides differed from those of saturated monoglycerides. Melting temperatures of 25 and 4.0 °C were measured for DOG and DLG, respectively (panels d and e of Figure 3, respectively). Cooling of the samples produced positive heat flow peaks at 14 and −5 °C, respectively. DSC plots of individual components of the lipid blend were normalized to the biological ratio (*21*) and overlaid (Figure 3f). When compared to the overlaid plot, the DSC plot of the lipid blend (Figure 3g) exhibited new melting peaks that shifted to lower temperatures (5, 20, and 63 °C). Instead of four crystallization peaks, the lipid blend contained two new peaks at 5 and 45 °C.

Fluorescence Characteristics of NR in the Lipid Blend. The fluorescence spectrum of NR is solvatochromic, with more hydrophobic solvents producing a shorter emission wavelength
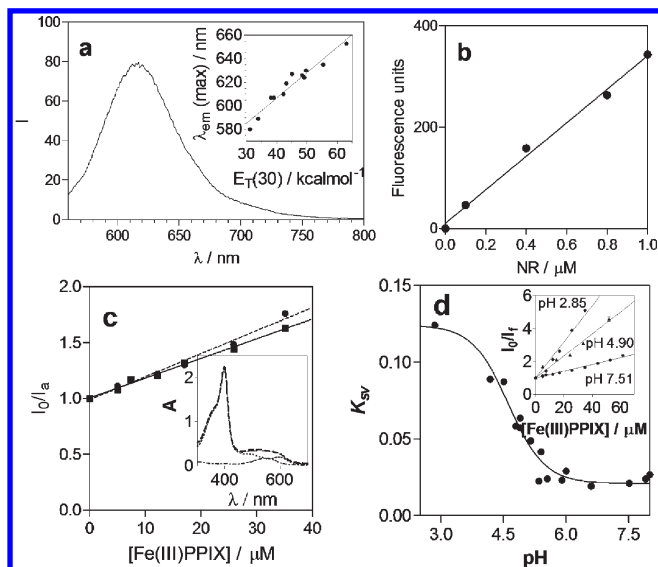
FIGURE 4: Fluorescence characteristics of NR in SNLDs and effects of Fe(III)PPIX. A typical bulk fluorescence emission spectrum of NR in SNLDs dispersed in aqueous solution (pH 7.51, 25 °C, 0.02 M HEPES buffer). The excitation wavelength is 540 nm. The inset shows the correlation ($r^2 = 0.94$) between the emission wavelength maximum of NR and the Dimroth−Reichardt hydrophobicity parameter $E_T(30)$ (*33*). The solvents are dodecane, toluene, ethyl acetate, chloroform, acetone, dimethylformamide, dimethyl sulfoxide, 2-propanol, pentanol, butanol, methanol, and water [from lowest to highest $E_T(30)$, respectively]. (b) The fluorescence intensity of NR exhibits a linear dependence on concentration in acetone up to at least 1 μM. The measurements were performed in a 1 cm quartz cuvette using a Varian Cary Eclipse UV−visible spectrofluorimeter. (c) Stern−Volmer plots for NR in SNLD at 25 (—) and 45 (---) °C. The increase in slope (K_{SV}) from 0.0185 to 0.0218 mM^{-1} is small but significant (with 95% confidence intervals of 0.0173−0.0197 and 0.0205−0.0231 mM^{-1}, respectively). The inset shows absorbance spectra of Fe(III)PPIX and NR in methanol. These are spectra for 33 μM Fe(III)PPIX (···) and 5 μM NR (·-·), the sum of these two spectra (---), and the spectrum of a mixture of 33 μM Fe(III)PPIX and 5 μM NR that is identical to the sum of the component spectra illustrating that neither spectrum changes as a result of mixing. (d) There is a significant increase in quenching constant K_{SV} (in units of mM^{-1}) with a decrease in the pH for NR in SNLDs dispersed in aqueous solution at 25 °C. The inset shows typical Stern−Volmer plots at pH 7.51, 5.0, and 2.85.

maximum [$\lambda_{em}(max)$] than more hydrophilic solvents (*24*). Examination of $\lambda_{em}(max)$ for a range of solvents exhibits a linear dependence of this parameter on the $E_T(30)$ of the solvent, a measure of microscopic hydrophobicity (Figure 4a, inset). The spectrum of NR in SNLDs (Figure 4a) exhibits a $\lambda_{em}(max)$ of 617 nm, corresponding to an $E_T(30)$ of 45 ± 4 kcal/mol. This is slightly more polar than acetone (42.2 kcal/mol) but less polar than octanol (48.1 kcal/mol) (*33*). It also definitively demonstrates that NR is incorporated into the SNLDs and does not reside in the aqueous solution, confirming the observations of the microscopy studies.

Fe(III)PPIX Partitioning into Neutral Lipid Droplets. One leading hypothesis for hemozoin formation involves expitaxial nucleation at the lipid−water interface, extension of the crystal along the interface, and an interior movement of the hydrophobic crystal to the interior of the NLB (*26, 34, 35*). However, little is known about the partitioning of Fe(III)PPIX molecules into the lipid droplets. Using the unique selective neutral lipid staining property of NR, it has been possible to follow the partitioning of soluble Fe(III)PPIX into SNLDs (*18, 24*). Fluorescence calibration measurements reveal a linear

relationship between the concentration of NR and the measured fluorescence intensity (up to 1 μM in a conventional cuvette and up to at least 12 μM when using a 96-well plate attachment) (Figure 4b). In all experiments presented here, the concentration of NR used in experimental measurements was well within the linear fluorescence range. The introduction of soluble Fe(III)-PPIX into an aqueous emulsion of the lipid blend containing NR resulted in concentration-dependent quenching of fluorescence with no shift in wavelength, demonstrating that NR is not displaced from the SNLDs into the aqueous phase by Fe(III)PPIX. This quenching was found to conform to the Stern−Volmer relationship up to at least 60 μM Fe(III)PPIX, indicating that the decrease in fluorescence intensity is a result of only one form of quenching in this range, either dynamic (collisional) or static quenching, because a mixed process gives rise to an upward deviation from linearity (*25*). The slope of the Stern−Volmer plot increases significantly with temperature (Figure 4c), and Fe(III)PPIX has no significant effect on the NR absorbance spectrum and vice versa (Figure 4c, inset). Collectively, these two observations convincingly suggest that dynamic rather than static quenching occurs in this case (*25*). The fact that the emission spectrum envelope does not change shape as it is quenched further indicates that the quenching is not simply a result of light absorbance by Fe(III)PPIX, because this would result in significant absorption at shorter wavelengths but little absorbance at longer wavelengths and would thus distort the shape of the emission spectrum. The slope of the Stern−Volmer plot, K_{SV}, is dependent on the pH of the aqueous medium (Figure 4d). Because K_{SV} is the product of the fluorescence lifetime of the fluorophore (τ_0) and the bimolecular quenching constant (k_q), it is not expected to change as a function of pH, because the hydrophobic interior of the NR-labeled SNLD is not likely to be altered by the pH of the aqueous medium. The most likely explanation for the increase in K_{SV} with a decrease in pH is therefore that the local concentration of Fe(III)PPIX in the SNLD increases with a decrease in pH because of increased partitioning of the partly protonated neutral form of Fe(III)-PPIX into the hydrophobic lipid. Indeed, the data can be fitted to a protonation model with a single pK_a of 4.62 ± 0.09, with a K_{SV} of 0.021 ± 0.003 μM^{-1} in the deprotonated form and a K_{SV} of 0.124 ± 0.007 μM^{-1} in the protonated form. Assuming that this difference arises solely as a result of the increased Fe(III)PPIX concentration in the SNLD particle in the case of the protonated form, this indicates a 6 ± 1-fold accumulation of the protonated relative to the uprotonated form of Fe(III)PPIX in SNLD. Unfortunately, the absolute log D_{lipid} cannot be evaluated from these data. However, measurement of octanol−water portioning of Fe(III)PPIX at pH 7.51 where it is soluble in both media indicates a log D_{OW} of ∼1.8. In combination, these data suggest an approximate log P for Fe(III)PPIX in its neutral form of ∼2.6.

This quenching of NR was visually corroborated using confocal microscopy. Immediately following the addition of Fe(III)-PPIX to NR-labeled SNLDs under physiological conditions, fluorescence quenching was observed (Figure 5a). In fact, the rate of partitioning of Fe(III)PPIX into the SNLDs was also found to be pH-dependent. Under pH conditions (2.3, 4.8, and 5.5) that more than span the expected range for the parasite DV (*36−38*), NR quenching observed at 50 s after the first addition of 500 μM Fe(III)PPIX was 74, 78, and 76%, respectively (Figure 5b). Interestingly, at pH 1.3, slightly less quenching was observed (26%), possibly because Fe(III)PPIX is entirely in its doubly
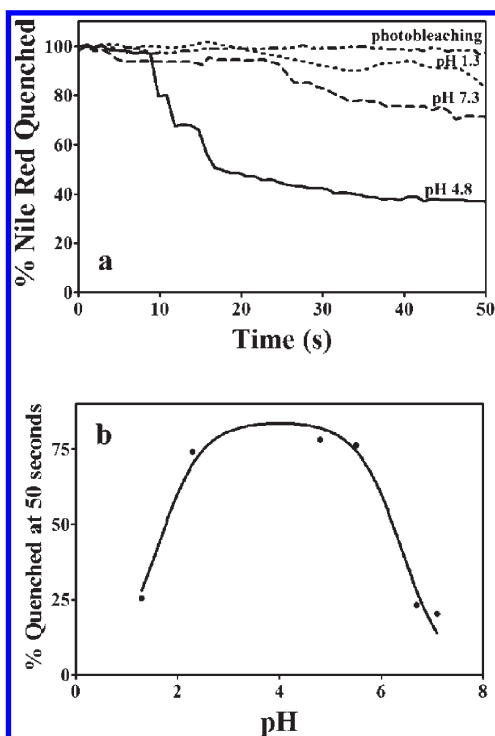
FIGURE 5: Photobleaching of NR and rates of Fe(III)PPIX quenching of NR-labeled SNLDs at pH 1.3, 7.3, and 4.8. At a pH similar to that of the DV of *P. falciparum* (4.8), Fe(III)PPIX rapidly partitions into SNLDs, indicated by quenching of NR (a). The dependence of the extent of NR quenching at 50 s after addition of Fe(III)PPIX illustrates a bell-shaped curve. At pH values where the two propionate groups of Fe(III)PPIX are predominately un-ionized or ionized, the rate of NR quenching is slower (b). In (a) 100% represents no quenching and 0% represents complete quenching.

protonated cationic form at this pH value. Likewise, significantly less quenching was observed (at 50 s) for pH 6.7, 7.3, and 8.1, respectively, where the NR quenching was only 23, 20, and 28%, respectively. At 150 s, the percents of total quenching for samples incubated at pH 2.3, 4.8, and 5.5 approach their maximum values (90, 92, and 94%, respectively). These values do not increase significantly at 200 s. For quenching at pH 4.8, a final Fe(III)-PPIX concentration of 220 μM was required to quench the interior of the NR-labeled SNLD. Note that this value reflects the overall amount of Fe(III)PPIX introduced into the SNLD solution and not the amount of Fe(III)PPIX localized within the SNLD.

At 200 s, maximal quenching of 80, 89, 87, and 57% was observed for samples incubated at pH 1.3, 6.7, 7.3, and 8.1, respectively. Location specific monitoring of fluorescence intensity during quenching experiments displayed selective localization of Fe(III)PPIX. Regions with no lipid present measured no significant changes in fluorescence. To ensure that the quenching effect was not due to photobleaching, the fluorescence intensity of labeled SNLDs was monitored. Mild quenching, specifically, a reduction of 2.0% in fluorescence intensity units, was measured after 50 s (Figure 5a) and 23% at 200 s, suggesting that drastically decreased fluorescence intensities of SNLDs were indeed a consequence of the addition of Fe(III)PPIX and not photobleaching. To confirm that the continual introduction of Fe(III)PPIX did not disrupt quenching measurements, Fe(III)PPIX was also added once to the NR-labeled SNLD suspension to produce a final Fe(III)PPIX concentration of 200 μM. Maximal quenching of this sample was still observed at 200 s; however, a slower rate of partitioning was observed. At the 50 s time point, only 40% quenching was observed.
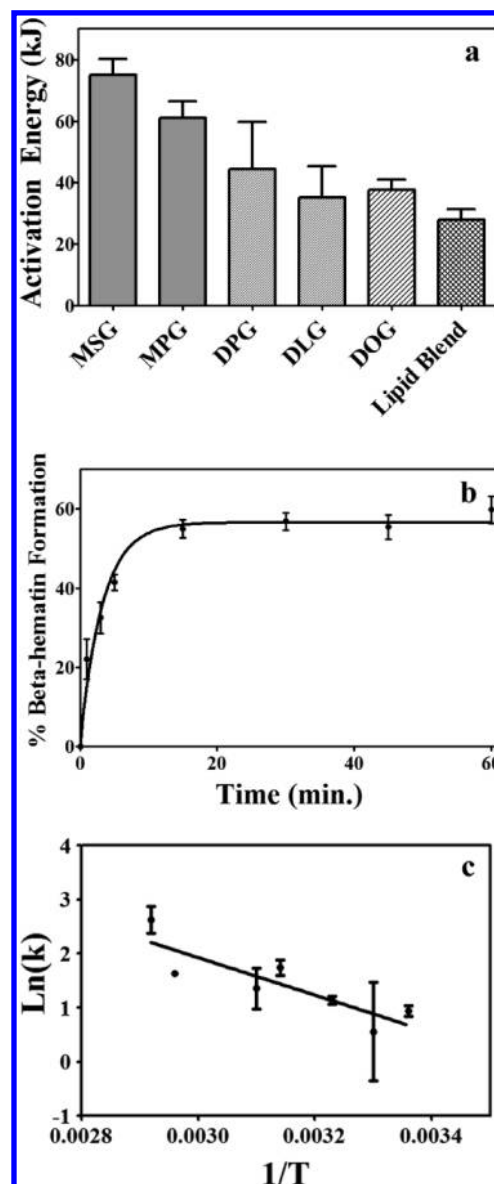

FIGURE 6: Kinetics of β-hematin formation. (a) Molar activation energies of β-hematin formation in the presence of the individual lipids and the blend. The error bars correspond to the standard error of the mean for three independent determinations. (b) Formation of β-hematin in the presence of SNLDs at pH 4.8 and 37 °C. The lipid droplets were suspended in citric buffer. The solid lines are best fits of three independent runs to a first-order kinetic equation. (c) Arrhenius plot for β-hematin formation in SNLDs at pH 4.8 in citric buffer.

Kinetics of β-Hematin Formation. SNLDs successfully promote β-hematin formation under physiologically relevant conditions (37 °C and pH 4.8) with a half-life ($t_{1/2}$) of 1.9 ± 0.01 min (Figure 6b). The activation energies of β-hematin formation mediated by SNLDs and each of the individual component lipids were determined from Arrhenius plots. An examination of activation energy revealed that monoglycerides exhibit energy barriers higher than those of diglycerides. MSG and MPG have calculated values of 74.8 ± 5.3 and 60.4 ± 7.1 kJ/mol, respectively, while DLG, DPG, and DOG exhibited lower values of 44.5 ± 15.4, 35.2 ± 9.4, and 37.7 ± 3.3 kJ/mol, respectively (Figure 6a). When the individual lipids are combined, the lipid blend revealed a much lower activation energy barrier of 27.8 ± 3.4 kJ/mol (Figure 6a,c). To evaluate the statistical significance of these relationships, *t* test analyses were

performed. Mean activation energies for the blend compared to those of MSG and MPG revealed differences at the 99.8% ($p = 0.002$) and 99.3% ($p = 0.007$) confidence levels, suggesting the observed differences between the blend and monoglycerides are statistically significant. Similar observations were calculated for blend with DOG and blend with DPG with 98% ($p = 0.02$) and 93% ($p = 0.07$) confidence levels, respectively. t test evaluation for blend with DLG revealed a difference at the 86% confidence level ($p = 0.14$).

DISCUSSION

Most eukaryotic cells contain cytosolic NLBs that are hypothesized to participate in energy storage (*20*, *39*). However, the presence of neutral lipid nanospheres in the DV of *Plasmodium* as well as the association of NLBs with the DV suggests that these neutral lipids may have a role in hemozoin formation, a process that occurs within this organelle. In this study, experimental data support the hypothesis that neutral lipid nanospheres within the DV possibly related to lipid bodies associated with the DV not only are the location of in vivo hemozoin formation but are also essential for the survival of the parasite by functioning as a time and site specific mediator of heme detoxification. Previous studies of SNLDs formed through sonication reported successful mediation of β-hematin formation (*18*). Recently, interfacial studies revealed crystal formation at a biologically compatible rate ($t_{1/2} \approx 2$ min) (*26*, *35*). In this study, the neutral lipid blend in the ratio reported by Sullivan and co-workers to be present in the parasite (4:2:1:1:1 MSG:MPG:DOG:DLG:DPG ratio) (*21*) was shown to support β-hematin formation by pXRD, FTIR, SEM, and TEM under biologically realistic conditions.

This lipid blend was found to spontaneously assemble into an emulsion with the lipid dispersed in a form resembling lipid droplets. These SNLDs displayed physical properties (i.e., spherical droplets with diameters in the range of hundreds of nanometers to a few micrometers) similar to those of their in vivo counterparts (*18*, *21*), rendering them useful for investigation of their role in hemozoin formation. Initially, it was thought that surface charges on the lipid droplets arising from noncovalent interactions with ions might provide a driving force for hemozoin nucleation; however, ζ potential measurements revealed that such interactions do not appear to occur, because all of the component lipids have values of <10 mV. In fact, the data suggest that the emulsions probably flocculate, a process in which the droplets coagulate, but retain their individual integrity. Such flocculated systems may then undergo coalescence, in which the interface between droplets is lost and single, larger droplets form (*28*). This would account for the SNLD size distribution that we have previously demonstrated (*26*) and the fairly large standard deviations in ζ potential.

The polarity of this lipid environment was found to lie between that of acetone and that of octanol as determined by the fluorescence emission peak maximum position of NR that occurs at 616 nm. It is notable that in *P. falciparum*, Jackson et al. observed weak fluorescence of NR with a wavelength maximum at 615 nm from the region immediately surrounding the hemozoin (*18*). At the time, this was ascribed to membrane material, but our findings suggest that it may well arise from the lipid spheres in which hemozoin is now known to form. By contrast, the interior of lipid bodies in the proximity of the DV is much more hydrophobic, giving a NR emission maximum of 590 nm (*18*).

The SNLD provides a unique crystallization environment that differs from that of its individual components. The melting properties revealed by DSC of the lipid blend are not merely an overlay of the phase transitions of each individual component. The interactions of the five neutral lipids produce two new crystallization and three new melting peaks, suggesting that the heterogeneous lipid population of the lipid blend facilitates a new molecular organization of the component lipids. A melting temperature shift to lower temperature suggests that less interaction is occurring between lipid molecules in the SNLD than in homogeneous samples. This is evident in a comparison of melting temperatures between mono- and diglycerides. In saturated lipids (MSG and MPG), the measured melting temperature is higher than that of unsaturated DLG and DOG. This is likely a result of the presence of double bonds in the unsaturated lipids. These "kinks" will weaken the alignment of the hydrocarbon chains, producing a more fluid packing environment. Despite the lipid blend being composed of a 7:2 ratio of monoglycerides to diglycerides, the presence of DOG and DLG reduces the primary melting peak. This lower melting point suggests that less stable or fewer interactions between lipid molecules are present in the SNLDs, which may result in more fluid and less oriented packing.

The new organization of lipids in the SNLD is not entirely unexpected given the differences in the number of free glycerol hydroxyl groups and acyl groups in monoglycerides versus diglycerides and in the degree of saturation of hydrocarbon chains of the components of the lipid blend. It has previously been demonstrated that the temperatures at which lipids undergo phase transitions are dependent upon the headgroup, the hydrocarbon chain length, and the degree and type of unsaturation present (*40*). For example, the addition of double bonds, as is the case with DOG and DLG, reduces the number of hydrophobic interactions between lipid molecules, thereby creating weaker dispersion interactions. Berlin and Sainz's DSC examination of phase transitions and molecular orientation in the liquid state of sonicated dispersions of neutral lipids reported that the positioning of acyl moieties in glycerolipids reduces the fluidity of dispersed lipid micelles (*31*). The authors attributed this restriction in mobility to the interactions between adjacent acyl chains. By the same reasoning, lipid droplets composed of homogeneous monoglycerides (MSG or MPG) are likely to exhibit more surface rigidity than lipid droplets composed of a heterogeneous composition, such as the lipid blend. The diversity in saturation of the components of the lipid blend will also contribute to the overall packing of the lipids in the lipid droplets, because unsaturated hydrocarbon chains do not pack as well as saturated chains. Together, the DSC data demonstrate that the SNLDs are partly molten, a fact that might play a significant role in the biological function of the blend in hemozoin formation.

To explore the partitioning of Fe(III)PPIX into SNLDs, we used the hydrophobic dye, NR. Conveniently, soluble Fe(III)PPIX was observed to be capable of quenching NR fluorescence. Temperature-dependent Stern–Volmer plots that show an increasing level of quenching with increasing temperature and a lack of sensitivity of the ground electronic state to interaction of NR with Fe(III)PPIX indicate that this is a result of collisional (dynamic) quenching (*25*). The combination of the pH dependence of NR quenching by Fe(III)PPIX and octanol–water partitioning of Fe(III)PPIX at pH 7.51 suggests that an ~400-fold partitioning of the neutral form of Fe(III)PPIX into SNLDs relative to the aqueous medium might be expected. This phenomenon was visualized by confocal microscopy as a diminishing

of fluorescence upon the addition of Fe(III)PPIX. In previous studies, TEM images of soluble Fe(III)PPIX introduced into synthetic lipid droplets composed of MPG showed the localization of electron dense matter surrounding the lipid droplets (26). However, in the absence of elemental imaging, it could not be confirmed that this electron dense material was indeed Fe(III)PPIX. In this study, confocal microscopic studies confirmed that Fe(III)PPIX spontaneously localizes to SNLDs under physiologically relevant conditions. Visually, a dramatic reduction in the fluorescence intensity of the NR-labeled lipid blend was observed upon introduction of Fe(III)PPIX (see the Supporting Information for real-time video imaging). Further addition of Fe(III)PPIX resulted in almost complete quenching of the droplet fluorescence. This may be the first visual, real-time, evidence of partitioning of heme into neutral lipid droplets. Within the malaria parasite, heme is released as a consequence of hemoglobin degradation in a continuous manner. The immediate localization of these heme molecules in the DV lipid nanospheres would be expected to encourage rapid crystallization of hemozoin. However, in vivo transport mechanisms remain unclear. No additional mediator was introduced to facilitate the trafficking of Fe(III)PPIX in this study. However, the same spontaneous localization may not exist within the complex environment of the DV.

The rate and extent of partitioning of Fe(III)PPIX into the SNLDs observed using confocal microscopy appear to be pH-dependent and seemingly parallel conditions required for β-hematin formation (26, 41, 42). In a pH range that encompasses that which promotes hemozoin formation in vivo (pH ~2.3–6.5), Fe(III)PPIX molecules partition rapidly into the SNLDs. Outside this range (pH 1.3, 6.7, 7.3, and 8.1), the initial (50 s) quenching was dramatically weaker. These observations can be attributed to the protonation state of Fe(III)PPIX. At low pH (< 2.0), both propionates of Fe(III)PPIX are protonated and a water molecule is present as the axial ligand. In this environment, an overall charge of +1 substantially decreases the partitioning of Fe(III)PPIX into the SNLDs. Between pH 2.3 and 5.5, one propionate is presumably deprotonated, producing an overall neutral state that allows Fe(III)PPIX to enter the SNLDs to a greater extent. From pH 5.5 to 7.5, both propionates are likely ionized, with the water axial ligand remaining protonated and resulting in an overall charge of −1. Fe(III)PPIX again cannot easily partition strongly into the lipid. At pH > 7.5, the axial ligand is OH^- and the overall charge is −2, further inhibiting Fe(III)PPIX from entering the lipid. Interestingly, over a longer time period, there is a further increase in the level of Fe(III)PPIX uptake under these conditions, indicating that the rate of Fe(III)-PPIX partitioning is decreased. However, in the pH range of the DV, released heme will be able to rapidly enter lipid droplets to a large extent and convert to hemozoin, allowing the parasite to avoid the consequent heme toxicity. This observed pattern of partitioning of heme into the SNLDs illustrates the ability of lipid droplets to control the site of hemozoin formation during heme detoxification. Similar pH trends of heme partitioning were observed for maximal quenching. In addition, peripheral quenching, indicating that Fe(III)PPIX did not enter the interior of the SNLDs, was observed at pH 1.3 and 6.7 and higher pH values.

The introduction of Fe(III)PPIX into the SNLD suspension successfully produced β-hematin with a $t_{1/2}$ of 1.9 ± 0.01 min at 37 °C and pH 4.8, close to that reported for the malaria parasite DV (43). This rate of heme conversion is well within the maximal half-life of 40 min previously estimated to be the maximum permitted to account for the observation that free heme in the parasite is limited to at most 5% at 36 h in the life cycle (35). Such a rapid rate of conversion of heme by the corresponding lipid blend in the parasite DV would therefore account for the fact that non-Hz Fe(III)PPIX is undetectable (i.e., makes up less than 5% of total Fe) in the Mössbauer spectrum of late trophozoite stage parasites (44). This lipid-mediated process is vastly more efficient and faster than that previously reported for protein-mediated hemozoin formation. For example, Pandey et al. reported only ~1% conversion over 12 h in the presence of histidine rich protein 2 (HRP II) (45), while Jani et al. reported slightly more than 30% conversion over 20 min and ~10% conversion over 10 min in the presence of the so-called heme dimerization protein (HDP) (46).

Kinetic studies revealed that the degree of saturation of the lipids influences the activation energy of β-hematin formation. SNLDs composed of just DPG, DOG, or DLG displayed activation energies lower than those of monoglycerides (MSG or MPG). The difference in molecular packing of the lipid molecules may be responsible for these measured differences. As explained above, DLG and DOG exhibit greater fluidity at the lipid body surface. This loosely packed surface may allow for faster organization of Fe(III)PPIX molecules, resulting in the measured lower activation energy. In the case of the lipid blend, the incorporation of a heterogeneous lipid population apparently alters the surface properties of the lipid body, with the differences in hydrocarbon chain length, degree of saturation, and head-group polarity all contributing to a more fluid and corrugated surface (47) that is better able to template β-hematin formation. This surface may provide "pockets" for precursor heme dimers to intercalate and assemble, initiating hemozoin nucleation. Furthermore, the increase in packing fluidity may explain the complexity of the lipid blend associated with hemozoin in the parasite. If one type of lipid is sufficient to template hemozoin formation (26, 35), why does the parasite use a composition of five different lipid components? The answer is likely to be associated with the increase in surface energy associated with the template surface. This is evident in the observed lower activation energy. Additional studies that include the examination of lipid packing are critical for the further evaluation of this hypothesis. Given that lipid peroxidation typically occurs at methylene groups adjacent to double bonds (48), making saturated lipids less susceptible to oxidative damage than unsaturated lipids, the blend might also provide a means for the parasite to create an interface with hemozoin forming properties that resembles that of unsaturated lipids, while retaining a lipid mixture that is composed of almost 80% saturated lipids. In the strongly oxidative environment of the DV, this may slow degradation of the lipid nanospheres and the production of lipid peroxides.

CONCLUSIONS

This study has shown that Fe(III)PPIX spontaneously and rapidly accumulates in SNLDs at pH values close to those of the DV of *P. falciparum*. The neutral lipid blend reported to be present in the DV has unique properties that seem to strongly promote β-hematin formation by drastically lowering the activation energy of the process relative to lipid emulsions containing saturated monoglycerides. In particular, despite being composed largely of saturated mono- and diglycerides, it lowers the activation energy to a level similar to but even lower than that of the unsaturated diglyceride DOG. This suggests that the particular

composition of the blend plays a critical role in its biological function. Collectively, these findings strongly support the hypothesis that hemozoin formation is caused by lipid droplets (lipid nanospheres) in the DV. It is noteworthy that the time period reported for NLB production in vivo coincides with that of the blood feeding stage of the *P. falciparum* life cycle. Studies of the incorporation of [^{14}C]oleic acid into serum free medium by Palacpac et al. have shown that mono- and diglyceride synthesis begins to appear ~10 h into the parasite life cycle and continues to the early schizont stage, while there is rapid incorporation into triglycerides during the late trophozoite stage, probably corresponding to formation of the neutral lipid bodies seen to be associated with the DV (*49*). The relative abundance and localization of lipid bodies are stage-dependent (*23, 50*), with large numbers of lipid bodies found in the late trophozoite and early schizont stages of the intraerythrocytic cycle (*17, 50*). In addition, microscopic observations of lipid bodies during the course of intraerythrocytic development have been reported to reveal tiny NR fluorescent dots ($< 1 \mu m$) in the early ring stage. These dots increase in size ($\sim 2 \mu m$) as development proceeds to later stages (*50*). The overlapping of neutral lipid production and hemoglobin degradation is unlikely to be coincidental. Given that the formation of NLBs and neutral lipid structures in the DV is probably related to common pathways in the parasite, this may indicate that neutral lipids are important in sustaining parasite viability via heme detoxification through mediation of hemozoin formation.

SUPPORTING INFORMATION AVAILABLE

Confocal micrographs of NR-labeled SNLDs in the presence of Fe(III)PPIX. The left-hand panels show NR fluorescence from NR in lipid droplets prior to addition of Fe(III)PPIX. Careful addition of Fe(III)PPIX results in almost complete quenching of the NR signal at pH 4.8 (c) and 5.5 (d) but incomplete or no quenching at pH 1.3 (a), 2.3 (b) 6.5 (e), 7.3 (f), and 8.1 (g). A Quicktime movie showing fluorescence quenching of NR in SNLDs after addition of Fe(III)PPIX. This material is available free of charge via the Internet at http://pubs.acs.org.

REFERENCES

1. Zweytick, D., Athenstaedt, K., and Daum, G. (2000) Intracellular lipid particles of eukaryotic cells. *Biochim. Biophys. Acta 1469*, 101–120.
2. Rudzinska, M. A., Trager, W., and Bray, R. S. (1965) Pinocytic uptake and digestion of haemoglobin in malaria parasites. *J. Protozool. 12*, 563–576.
3. Goldberg, D. E., Slater, A. F. G., Cerami, A., and Henderson, G. B. (1990) Haemoglobin degradation in the malaria parasite *Plasmodium falciparum*: An ordered process in a unique organelle. *Proc. Natl. Acad. Sci. U.S.A. 87*, 2931–2935.
4. Loria, P., Miller, S., Foley, M., and Tilley, L. (1999) Inhibition of the peroxidative degradation of haem as the basis of action of chloroquine and other quinoline antimalarials. *Biochem. J. 339*, 363–370.
5. Kutner, S., Breuer, W. V., Ginsburg, H., Aley, S. B., and Cabantchik, Z. I. (1985) Characterization of permeation pathways in the plasma membrane of human erythrocytes infected with early stages of *Plasmodium falciparum*: Association with parasite development. *J. Cell. Physiol. 125*, 521–527.
6. Ginsburg, H., Kutner, S., Krugliak, M., and Cabantchik, Z. I. (1985) Characterization of permeation pathways appearing in the host membrane of *Plasmodium falciparum* infected red blood cells. *Mol. Biochem. Parasitol. 14*, 313–322.
7. Lew, V. L., Tiffert, T., and Ginsburg, H. (2003) Excess hemoglobin digestion and the osmotic stability of *Plasmodium falciparum*-infected red blood cells. *Blood 101*, 4189–4194.
8. Goldberg, D. E., Slater, A. F. G., Beavis, R., Chait, B., Cerami, A., and Henderson, G. B. (1991) Haemoglobin degradation in the human malaria pathogen *Plasmodium falciparum*: A catabolic pathway initiated by a specific aspartic protease. *J. Exp. Med. 173*, 961–969.
9. Fitch, C. D., and Kanjananggulpan, P. (1987) The state of ferri-protoporphyrin IX in malaria pigment. *J. Biol. Chem. 262*, 15552–15555.
10. Slater, A. F. G., Swiggard, W. J., Orton, B. R., Flitter, W. D., Goldberg, D. E., Cerami, A., and Henderson, G. B. (1991) An iron-carboxylate bond links the heme units of malaria pigment. *Proc. Natl. Acad. Sci. U.S.A. 88*, 325–329.
11. Bohle, D. S., Dinnebier, R. E., Madsen, S. K., and Stephens, P. W. (1997) Characterization of the products of the heme detoxification pathway in malarial late trophozoites by X-ray diffraction. *J. Biol. Chem. 272*, 713–716.
12. Klonis, N., Dilanian, R., Hanssen, E., Darmanin, C., Streltsov, V., Deed, S., Quiney, H., and Tilley, L. (2010) Hematin-hematin self-association states involved in the formation and reactivity of the malaria parasite pigment, hemozoin. *Biochemistry 49*, 6804–6811.
13. Pagola, S., Stephens, P. W., Bohle, D. S., Kosar, A. D., and Madsen, S. K. (2000) The structure of malaria pigment (β-haematin). *Nature 404*, 307–310.
14. Ziegler, J., Linck, R., and Wright, D. W. (2001) Heme aggregation inhibitors: Antimalarial drugs targeting an essential biomineralization process. *Curr. Med. Chem. 8*, 171–189.
15. Ancelin, M. L., and Vial, H. J. (1992) Saturable and non-saturable components of choline transport in *Plasmodium*-infected mammalian erythrocytes: Possible role of experimental conditions. *Biochem. J. 283*, 619–621.
16. Holz, G. G. J. (1977) Lipids and the malarial parasite. *Bull. W.H.O. 55*, 237–248.
17. Vielemeyer, O., McIntosh, M. T., Joiner, K. A., and Coppens, I. (2004) Neutral lipid synthesis and storage in the intraerythrocytic stages of *Plasmodium falciparum*. *Mol. Biochem. Parasitol. 135*, 195–207.
18. Jackson, K. E., Klonis, N., Ferguson, D. J. P., Adisa, A., Dogovski, C., and Tilley, L. (2004) Food vacuole-associated lipid bodies and heterogeneous lipid environments in the malaria parasite, *Plasmodium falciparum*. *Mol. Microbiol. 54*, 109–122.
19. Nawabi, P., Lykidis, A., Ji, D., and Haldar, K. (2003) Neutral-lipid analysis reveals elevation of acylglycerols and lack of cholesterol esters in *Plasmodium falciparum*-infected erythrocytes. *Eukaryotic Cell 2*, 1128–1131.
20. Coppens, I., and Vielemeyer, O. (2005) Insights into unique physiological features of neutral lipids in Apicomplexa: From storage to potential mediation in parasite metabolic activities. *Int. J. Parasitol. 35*, 597–615.
21. Pisciotta, J. M., Coppens, I., Tripathi, A. K., Scholl, P. F., Shuman, J., Bajad, S., Shulaev, V., and Sullivan, D. J. (2007) The role of neutral lipid nanospheres in *Plasmodium falciparum* heme crystallization. *Biochem. J. 402*, 197–204.
22. Hempelmann, E., Motta, C., Hughes, R., Ward, S. A., and Bray, P. G. (2003) *Plasmodium falciparum*: Sacrificing membrane to grow crystals? *Trends Parasitol. 19*, 23–26.
23. Palacpac, N. M. Q., Hiramine, Y., Seto, S., Hiramatsu, R., Horii, T., and Mitamura, T. (2004) Evidence that *Plasmodium falciparum* diacylglycerol acyltransferase is essential for intraerythrocytic proliferation. *Biochem. Biophys. Res. Commun. 321*, 1062–1068.
24. Greenspan, P., Mayer, E. P., and Fowler, S. D. (1985) Nile red: A selective fluorescent stain for intracellular lipid droplets. *J. Cell Biol. 100*, 965–973.
25. Lakowicz, J. R. (2006) Principles of fluorescence spectroscopy, 3rd ed., Springer Science and Business Media, New York.
26. Hoang, A. N., Ncokazi, K. K., de Villiers, K. A., Wright, D. W., and Egan, T. J. (2010) Crystallization of synthetic haemozoin (β-haematin) nucleated at the surface of lipid particles. *Dalton Trans. 39*, 1235–1244.
27. Riddick, T. M., and Ravina, L. A. (1970) Electrophoresis. *Ind. Eng. Chem. 62*, 70–73.
28. Washington, C. (1996) Stability of lipid emulsions for drug delivery. *Adv. Drug Delivery Rev. 20*, 131–145.
29. Ciani, L., Ristori, S., Salvati, A., Calamai, L., and Martini, G. (2004) DOTAP/DOPE and DC-Chol/DOPE lipoplexes for gene delivery: ζ potential measurements and electron spin resonance spectra. *Biochim. Biophys. Acta 1664*, 70–79.
30. Gunston, F. D., and Padley, F. B., Eds. (1997) Lipid technologies and applications, Marcel Dekker Inc., New York.
31. Berlin, E., and Sainz, E. (1986) Acyl chain interactions and the modulation of phase changes in glycerolipids. *Biochim. Biophys. Acta 855*, 1–7.

32. Krog, N. J. (2001) Crystallization properties and lyotropic phase behavior of food emulsifiers. In Crystallization processes in fats and lipid systems (Garti, N., and Sato, K., Eds.) pp 505−526, Marcel Dekker Inc., New York.

33. Reichardt, C. (1994) Solvatochromic dyes as solvent polarity indicators. *Chem. Rev. 94*, 2319–2358.

34. Solomonov, I., Osipova, M., Feldman, Y., Baehtz, C., Kjaer, K., Robinson, I. K., Webster, G. T., McNaughton, D., Wood, B. R., Weissbuch, I., and Leiserowitz, L. (2007) Crystal nucleation, growth, and morphology of the synthetic malaria pigment β-hematin and the effect thereon by quinoline additives: The malaria pigment as a target of various antimalarial drugs. *J. Am. Chem. Soc. 129*, 2615–2627.

35. Egan, T. J., Chen, J. Y.-J., de Villiers, K. A., Mabotha, T. E., Naidoo, K. J., Ncokazi, K. K., Langford, S. J., McNaughton, D., Pandiancherri, S., and Wood, B. R. (2006) Haemozoin (β-haematin) biomineralization occurs by self-assembly near the lipid/water interface. *FEBS Lett. 580*, 5105–5110.

36. Yayon, A., Cabantchik, Z. I., and Ginsburg, H. (1984) Identification of the acidic compartment of *Plasmodium falciparum*-infected human erythrocytes as the target of the antimalarial drug chloroquine. *EMBO J. 3*, 2695–2700.

37. Geary, T. G., Divo, A. D., Jensen, J. B., Zangwill, M., and Ginsburg, H. (1990) Kinetic modelling of the response of *Plasmodium falciparum* to chloroquine and its experimental testing *in vitro*. *Biochem. Pharmacol. 40*, 685–691.

38. Hayward, R., Saliba, K. J., and Kirk, K. (2006) The pH of the digestive vacuole of *Plasmodium falciparum* is not associated with chloroquine resistance. *J. Cell Sci. 119*, 1016–1025.

39. Murphy, D. J. (2001) The biogenesis and functions of lipid bodies in animals, plants and microorganisms. *Prog. Lipid Res. 40*, 325–438.

40. Chapman, D. (1968) Biological membranes, Vol. 1, Academic Press, New York.

41. Egan, T. J., Mavuso, W. W., and Ncokazi, K. K. (2001) The mechanism of β-hematin formation in acetate solution. Parallels between hemozoin formation and biomineralization processes. *Biochemistry 40*, 204–213.

42. Egan, T. J., and Tshivhase, M. G. (2006) Kinetics of β-haematin formation from suspensions in aqueous benzoic acid. *Dalton Trans.,* 5024–5032.

43. Hayward, R., Saliba, K. J., and Kirk, K. (2005) Mutations in *pfmdr1* modulate the sensitivity of *Plasmodium falciparum* to the intrinsic antiplasmodial activity of verapamil. *Antimicrob. Agents Chemother. 49*, 840–842.

44. Egan, T. J., Combrinck, J. M., Egan, J., Hearne, G. R., Marques, H. M., Ntenteni, S., Sewell, B. T., Smith, P. J., Taylor, D., van Schalkwyk, D. A., and Walden, J. C. (2002) Fate of haem iron in the malaria parasite *Plasmodium falciparum*. *Biochem. J. 365*, 343–347.

45. Pandey, A. V., Babbarwal, V. K., Okoyeh, J. N., Joshi, R. M., Puri, S. K., Singh, R. L., and Chauhan, V. S. (2003) Hemozoin formation in malaria: A two-step process involving histidine-rich proteins and lipids. *Biochem. Biophys. Res. Commun. 308*, 736–743.

46. Jani, D., Nagarkatti, R., Beatty, W., Angel, R., Slebodnick, C., Andersen, J., Kumar, S., and Rathore, D. (2008) HDP: A novel heme detoxification protein from the malaria parasite. *PLoS Pathog. 4*, e1000053.

47. Holman, K. T., Pivovar, A. M., Swift, J. A., and Ward, M. D. (2001) Metric engineering of soft molecular host frameworks. *Acc. Chem. Res. 34*, 107–118.

48. Cheng, Z., and Li, Y. (2007) What is responsible for the initiating chemistry of iron-mediated lipid peroxidation: An update. *Chem. Rev. 107*, 748–766.

49. Palacpac, N. M. Q., Hiramine, Y., Mi-ichi, F., Torii, M., Kita, K., Hiramatsu, R., Horii, T., and Mitamura, T. (2004) Developmental-stage-specific triacylglycerol biosynthesis, degradation and trafficking as lipid bodies in *Plasmodium falciparum*-infected erythrocytes. *J. Cell Sci. 117*, 1469–1480.

50. Mitamura, T., and Palacpac, N. M. Q. (2003) Lipid metabolism in *Plasmodium falciparum*-infected erythrocytes: Possible new targets for malaria chemotherapy. *Microbes Infect. 5*, 545–552.